

Figure 1: Schematic showing (a) the locations for EBSD scans and regular X-ray measurement and (b) the scheme of micro- hardness measurement on the HPT-processed discs.

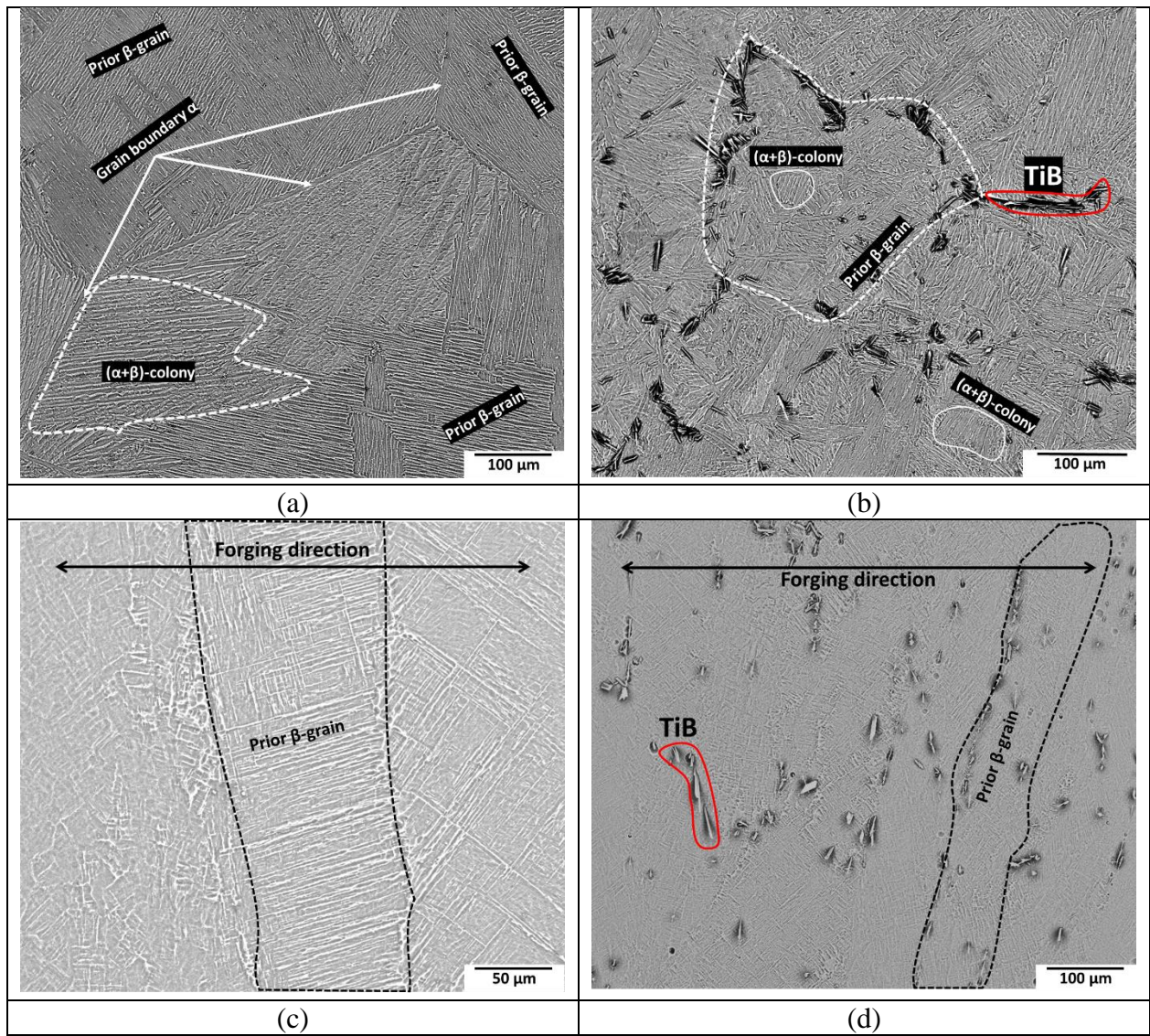
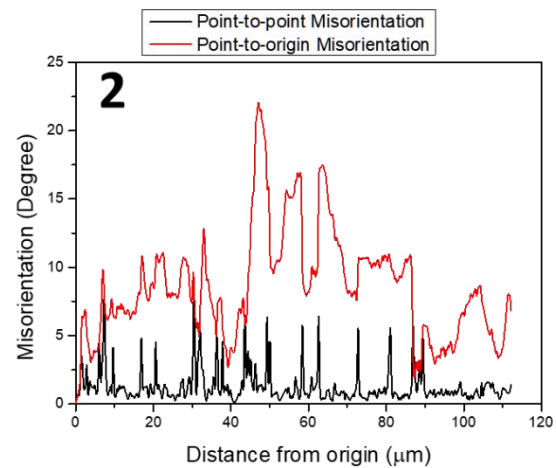
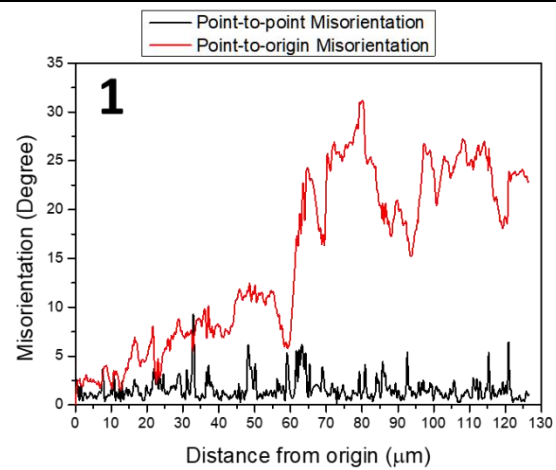
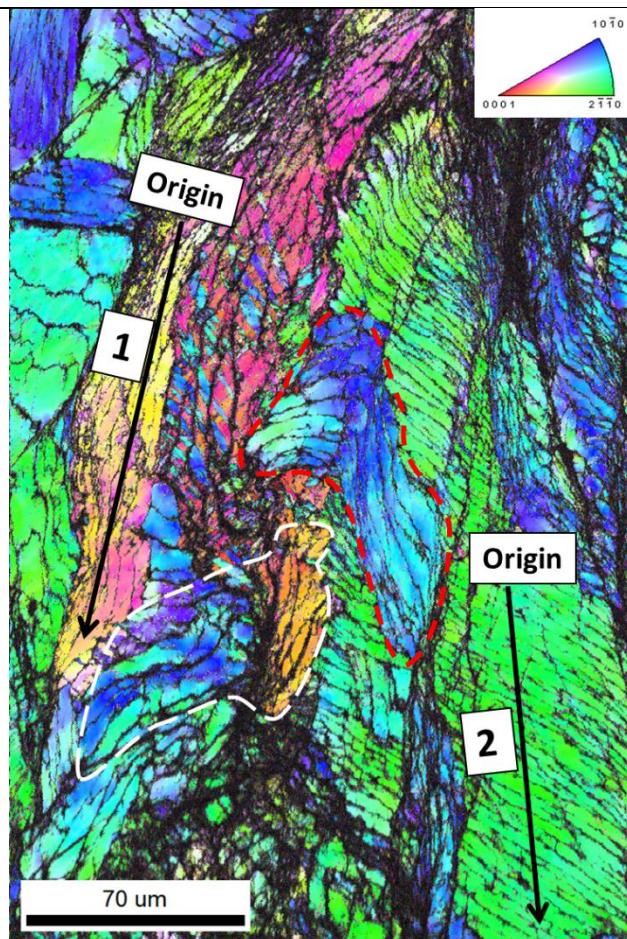
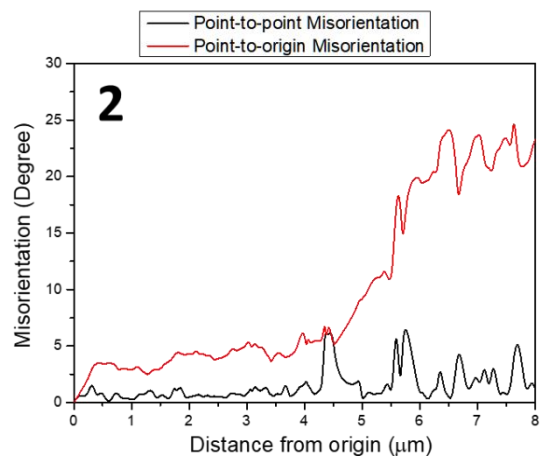
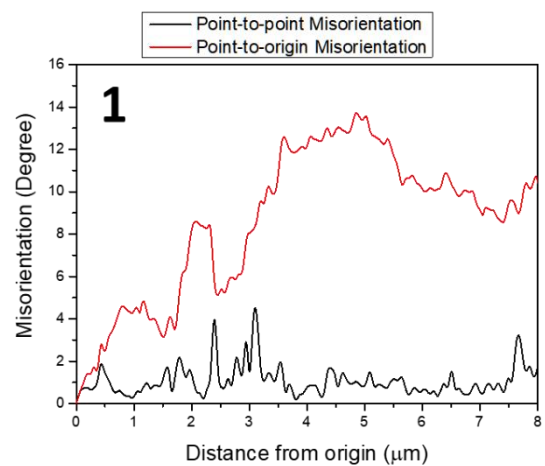
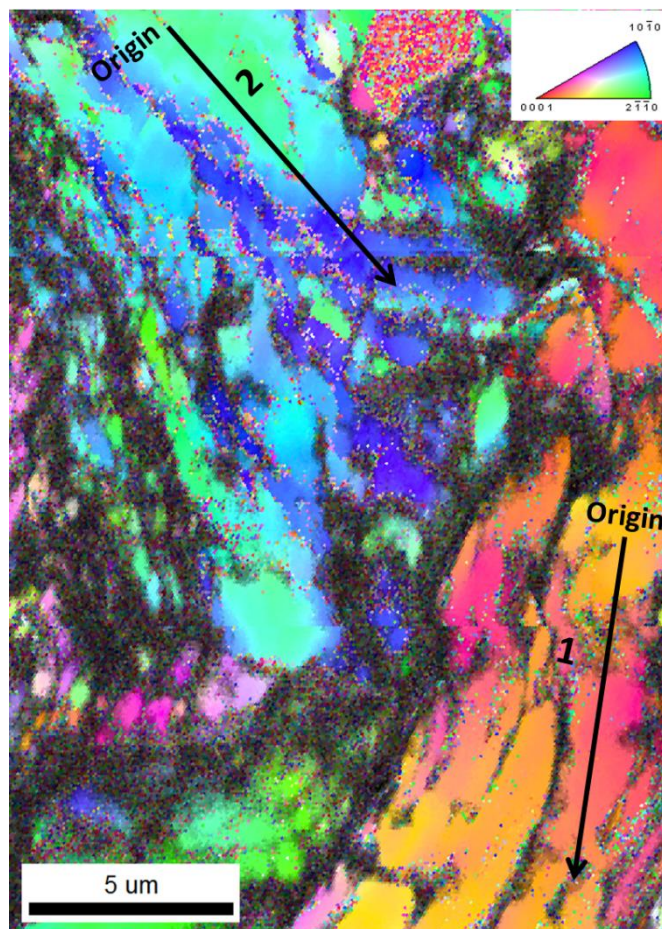


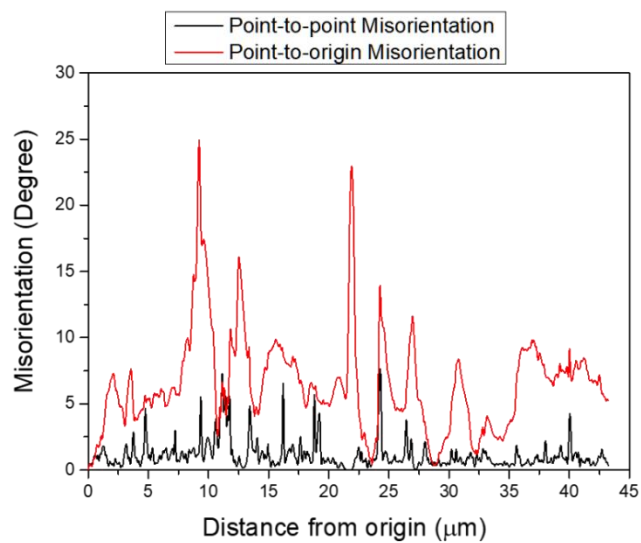
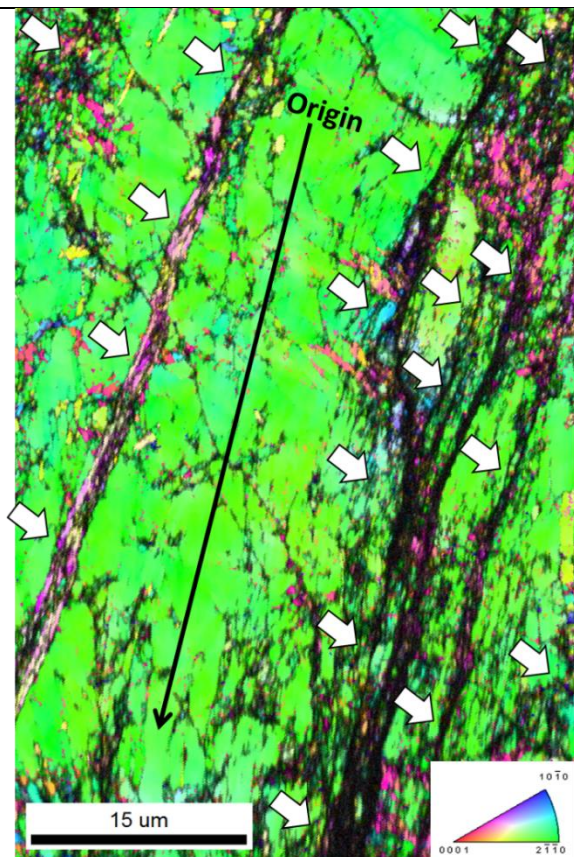
Figure 2: SEM images (BSE mode) showing starting microstructures (before HPT processing) for (a) Ti64-C, (b) Ti64+B-C, (c) Ti64-F and (d) Ti64+B-F alloys.



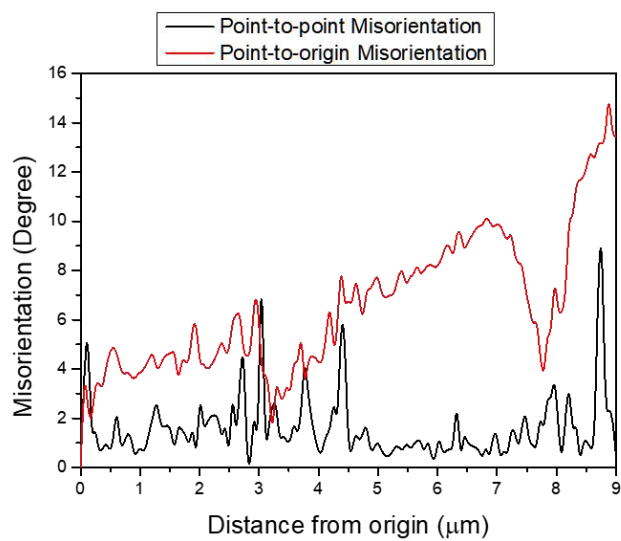
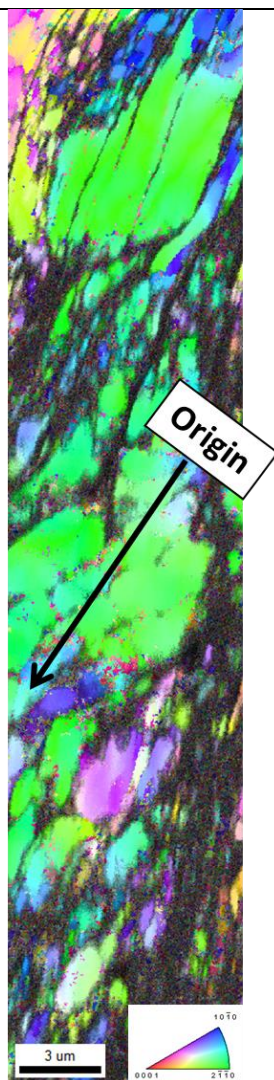
(a)



(b)



(c)



(d)

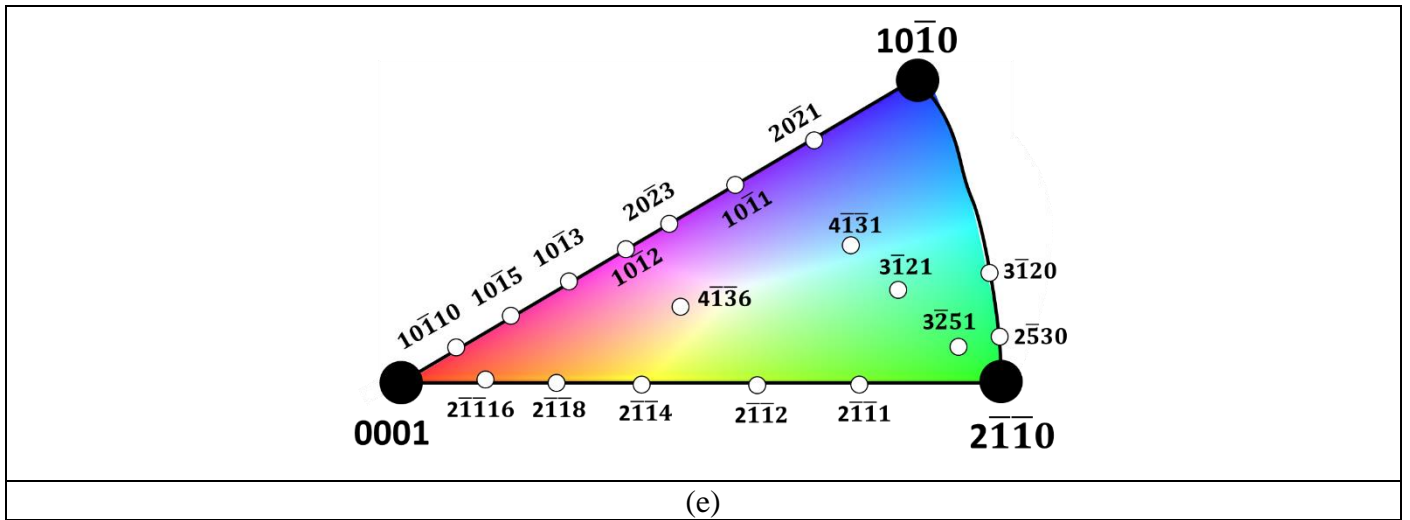
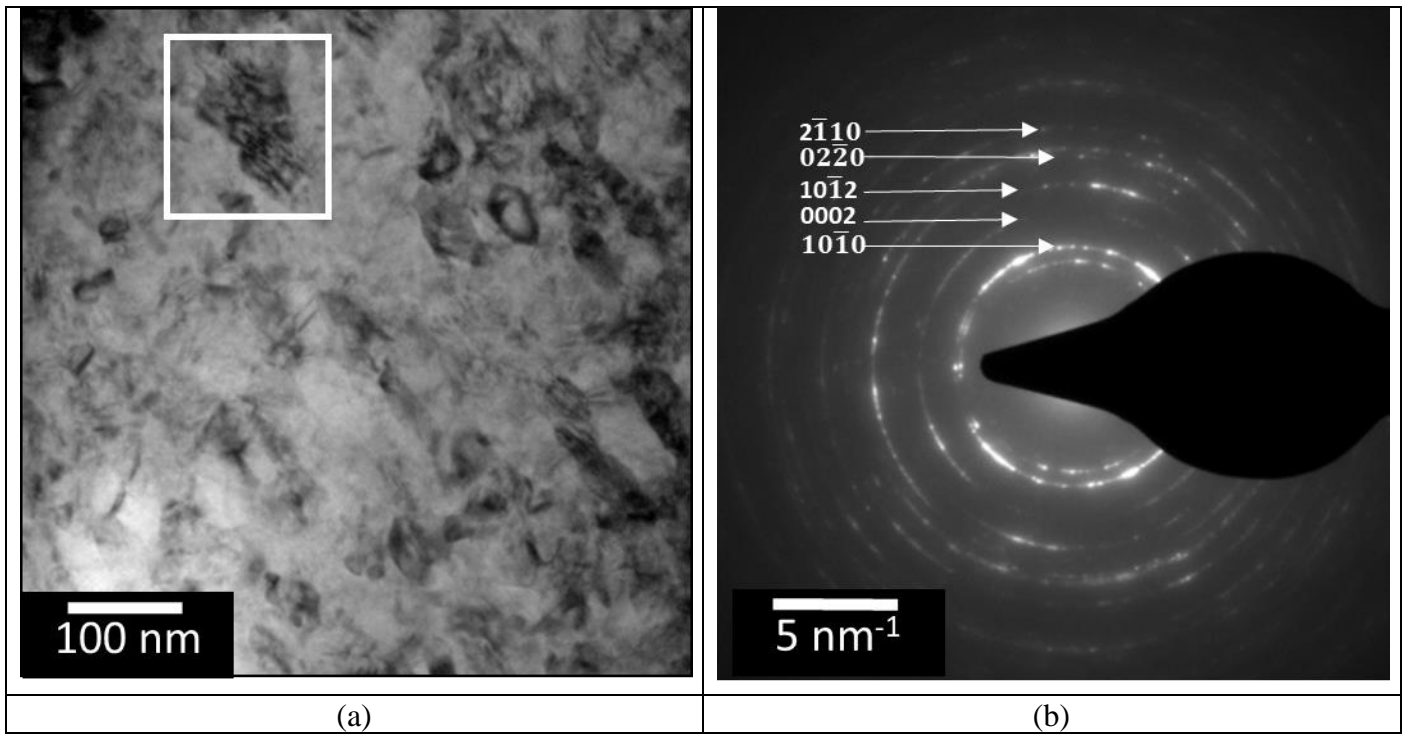
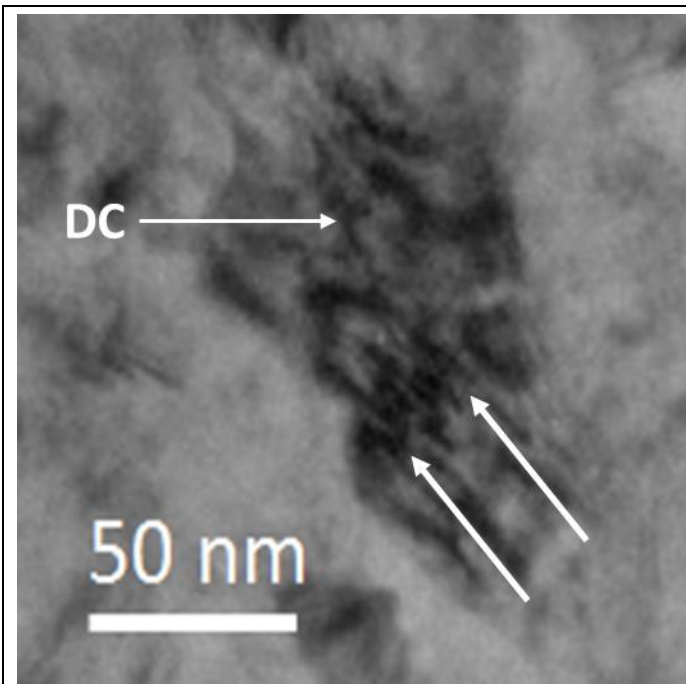
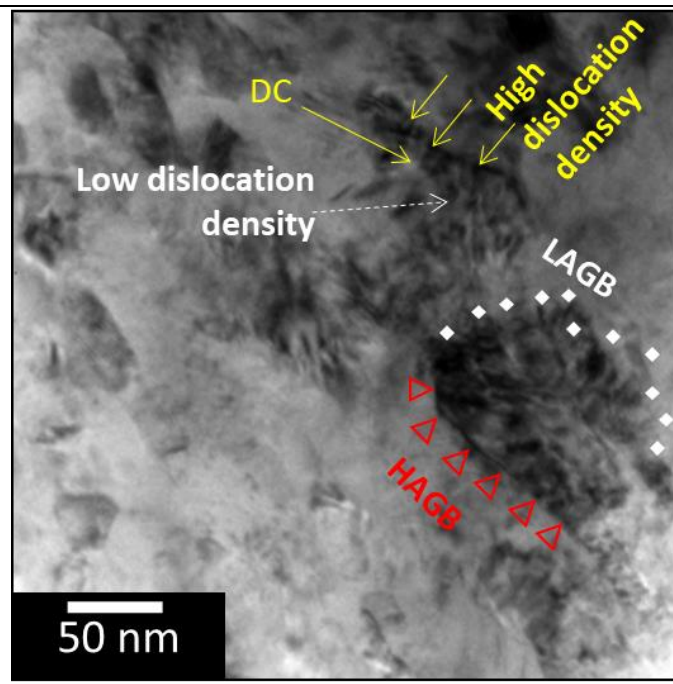


Figure 3: EBSD IPF maps (superimposed with image quality) showing microstructures of (a) Ti64-C, (b) Ti64+B-C, (c) Ti64-F, and (d) Ti64+B-F alloys after one HPT-rotation; (e) showing standard stereographic triangle superimposed with reference color triangle for hcp materials; it thus represents important directions and corresponding reference colors in EBSD IPF maps. Alongside IPF maps, the change in misorientation (on a point-to-point and point-to-origin basis) inside individual α -colonies is also plotted for different alloys.

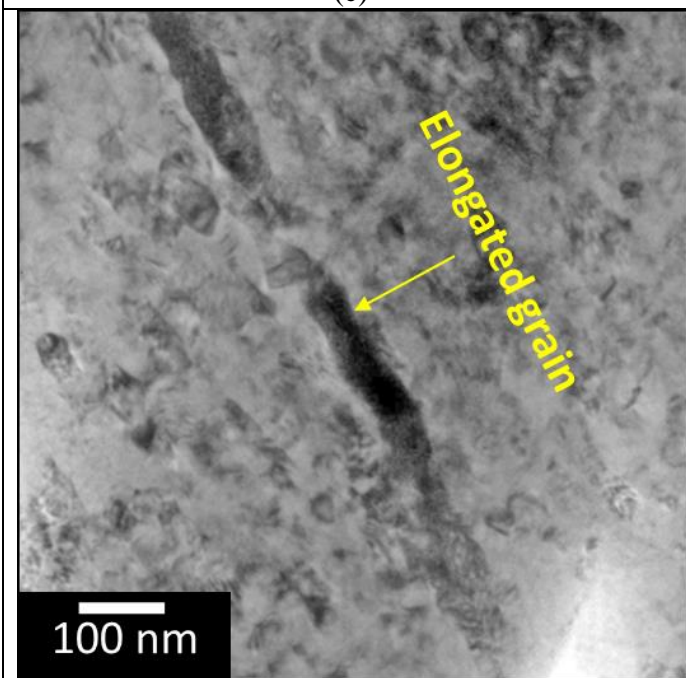




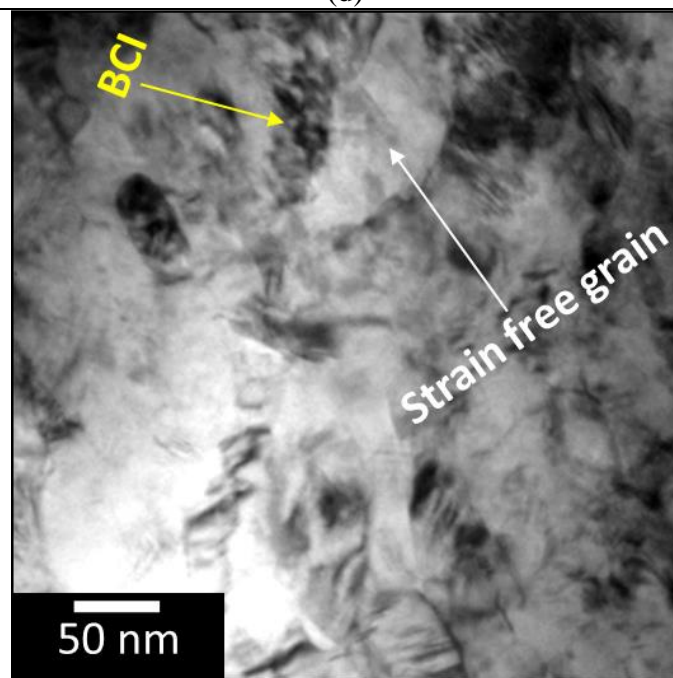
(c)



(d)



(e)



(f)

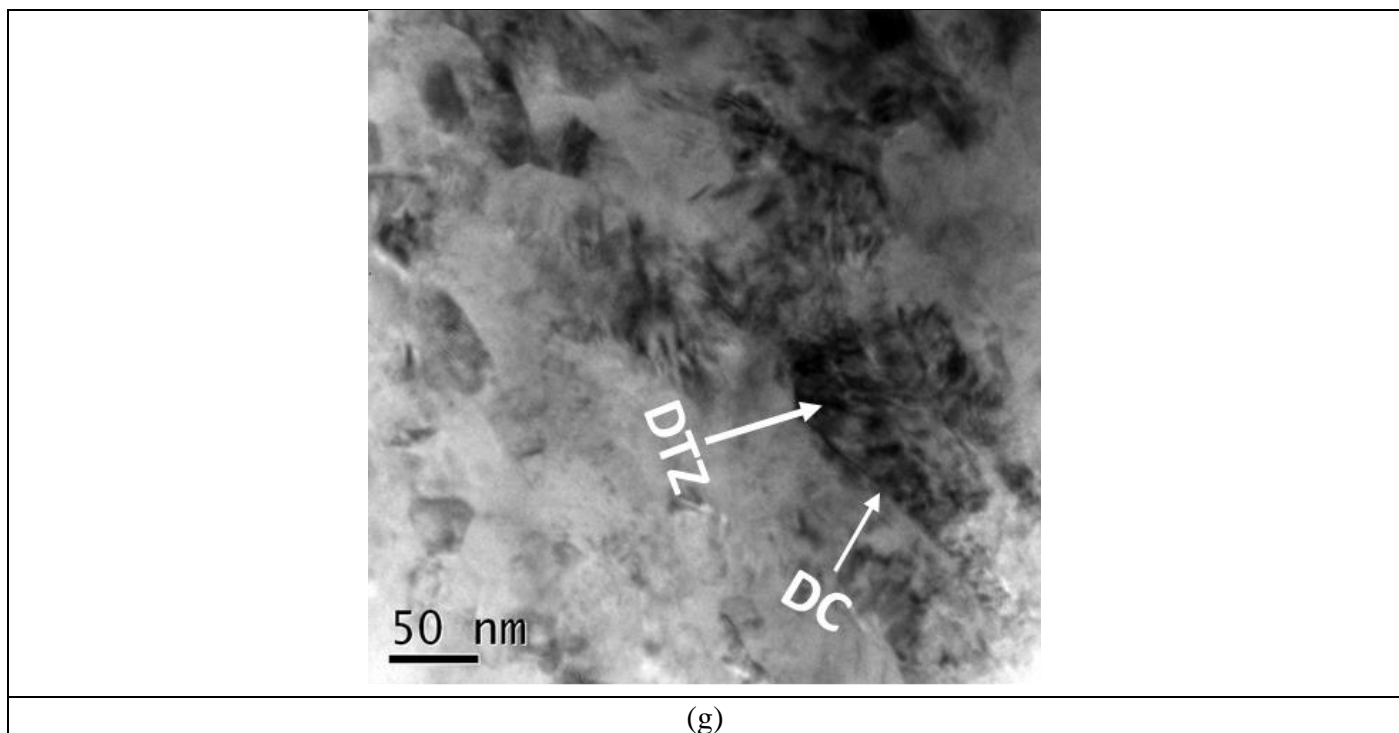
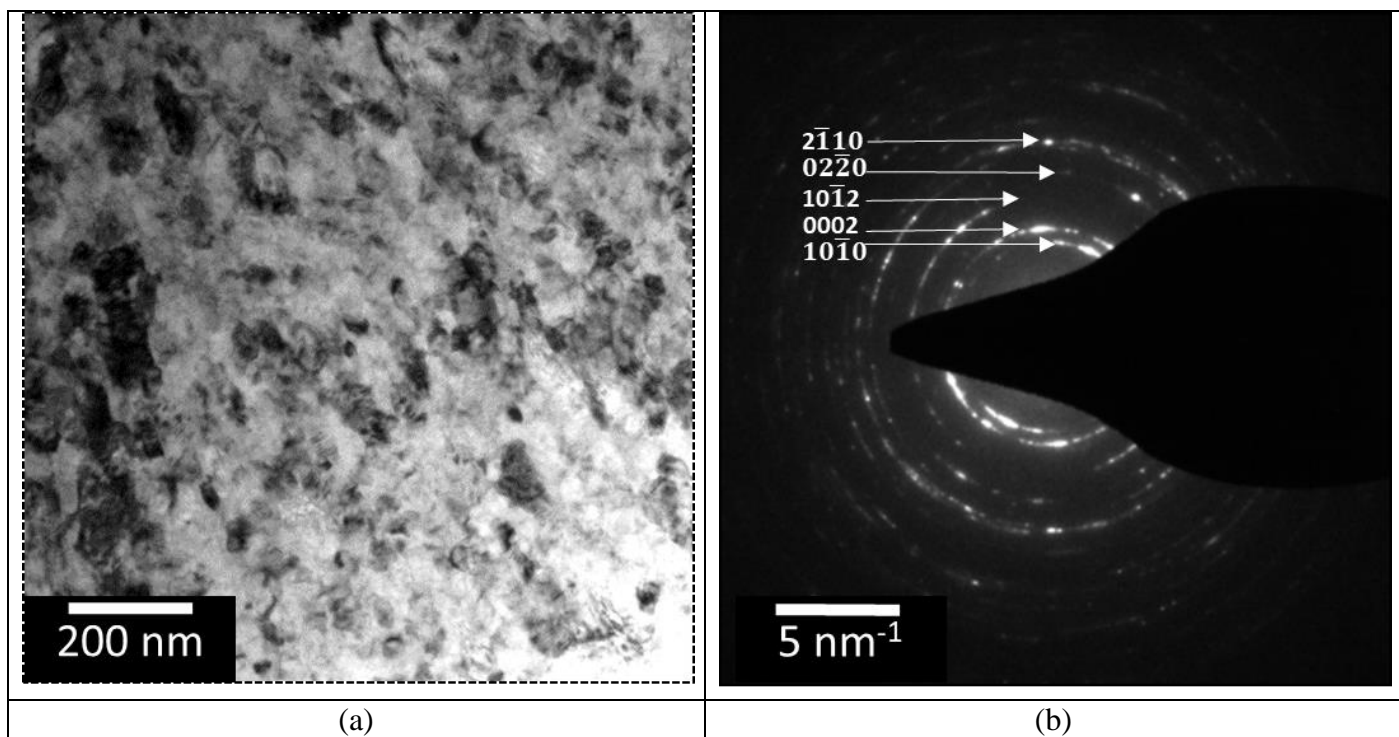
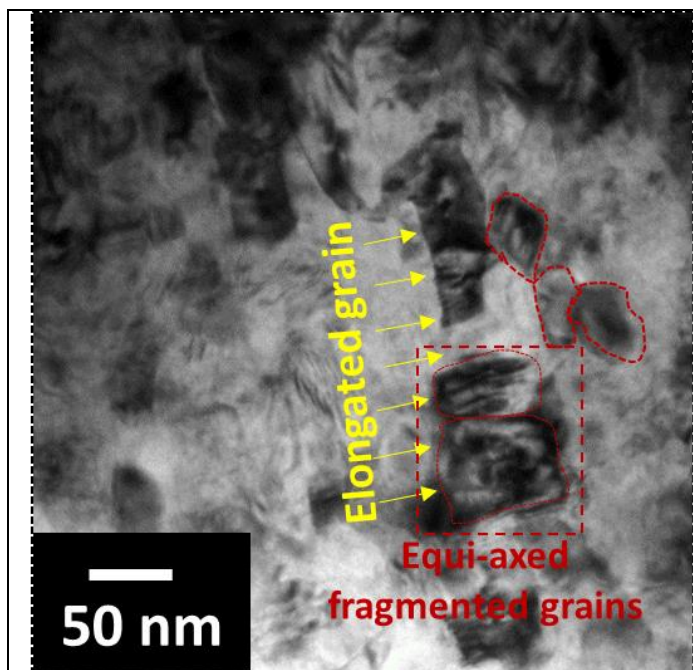
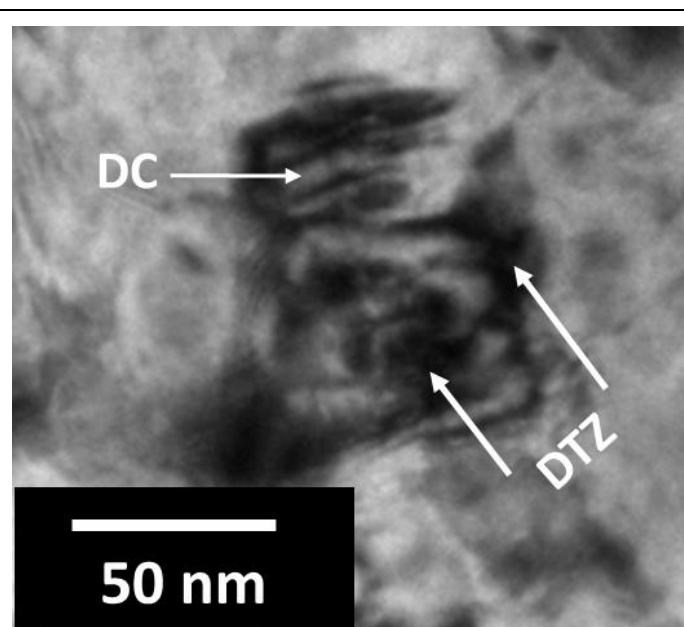


Figure 4: TEM micrographs (brightfield mode) showing (a), (c), (d) microstructure and (b) corresponding SAD pattern for Ti64-C alloy; (e), (f), (g) microstructures for Ti64+B-C alloy after 10 HPT-rotations. Important features and observation areas are marked in these micrographs.

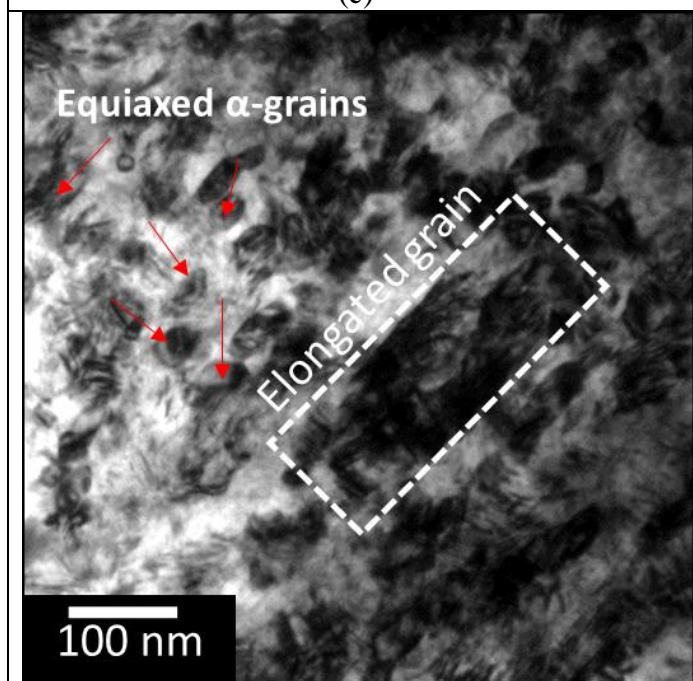




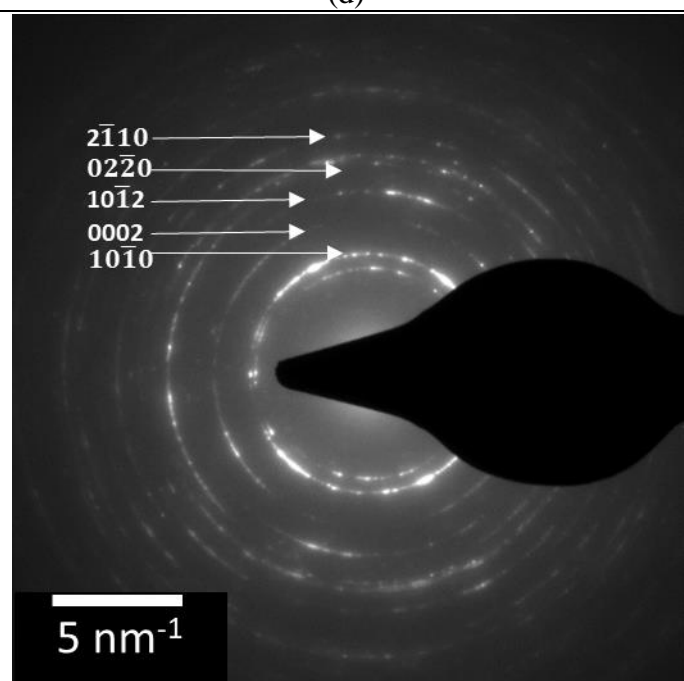
(c)



(d)



(e)



(f)

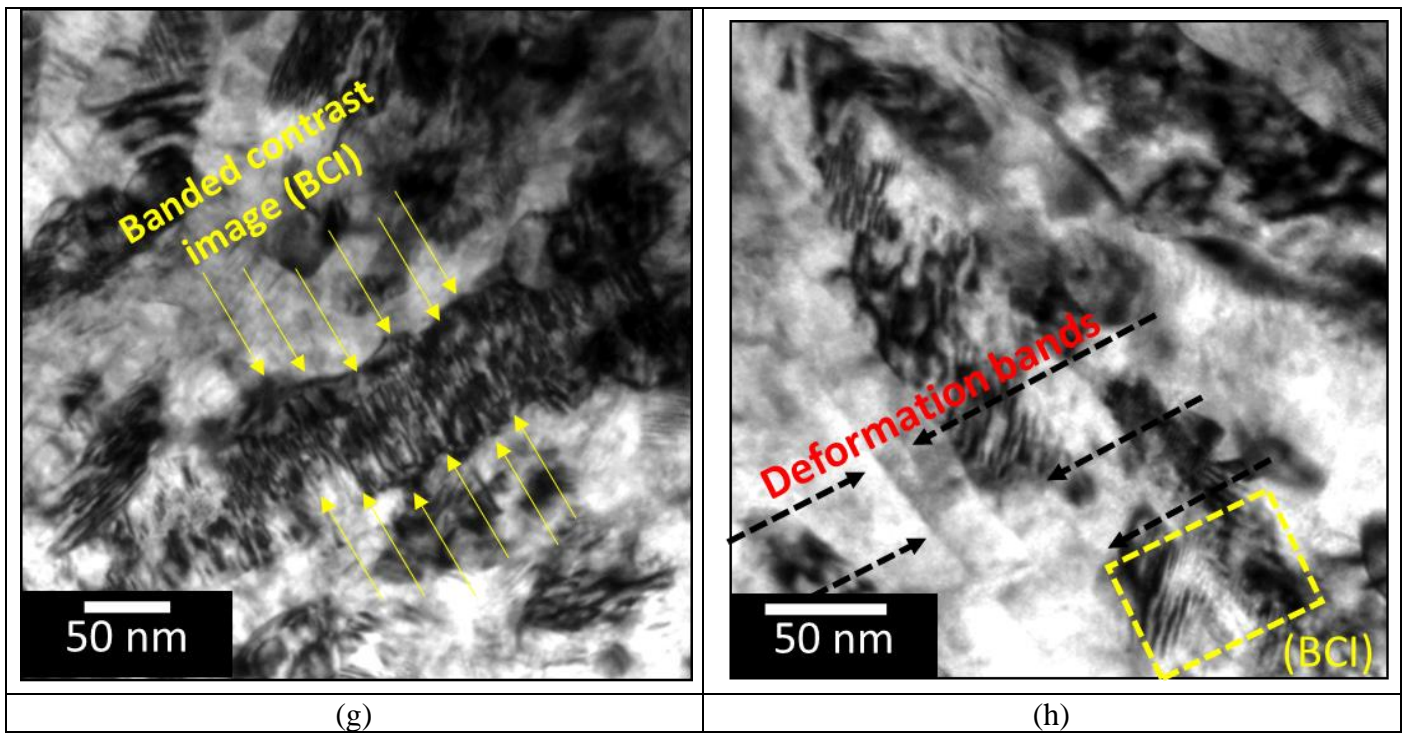


Figure 5: TEM images (brightfield mode) showing (a), (c), (d) microstructure and (b) SAD pattern for Ti64-F alloy; (e), (g), (h) microstructures and (f) SAD pattern for Ti64+B-F alloy after 10 HPT-rotations. Important features and observation areas are marked in the micrographs.

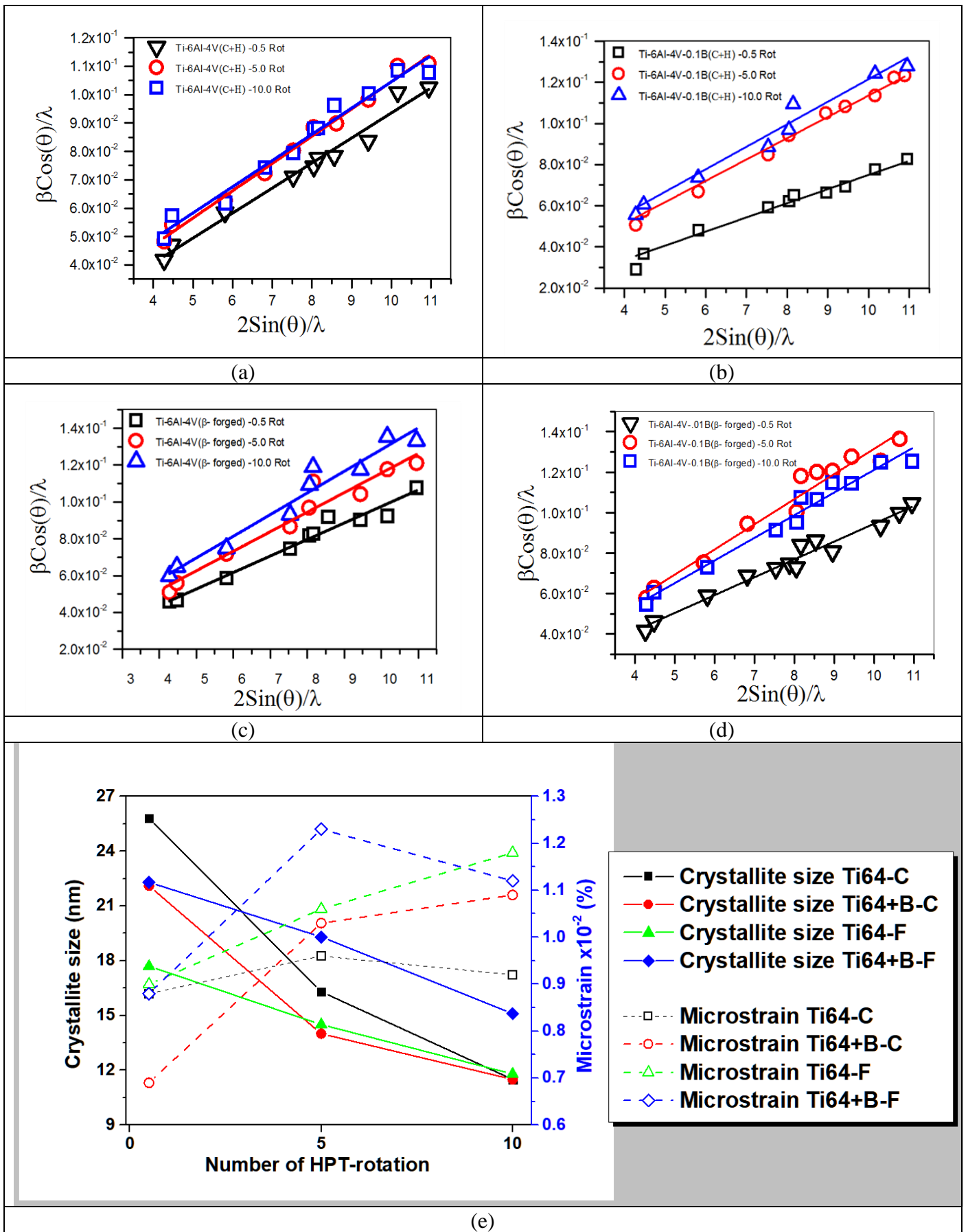


Figure 6: Classical Williamson-Hall plot showing the variation in FWHM with HPT-rotations for (a), (b) Ti64-C and Ti64+B-C alloys, respectively in as-cast condition and (c), (d) Ti64-F and Ti64+B-F alloys, respectively in β -forged condition; (e) variation in crystallite size and micro-strain calculated from W-H analysis with HPT-rotations for different alloys and conditions.

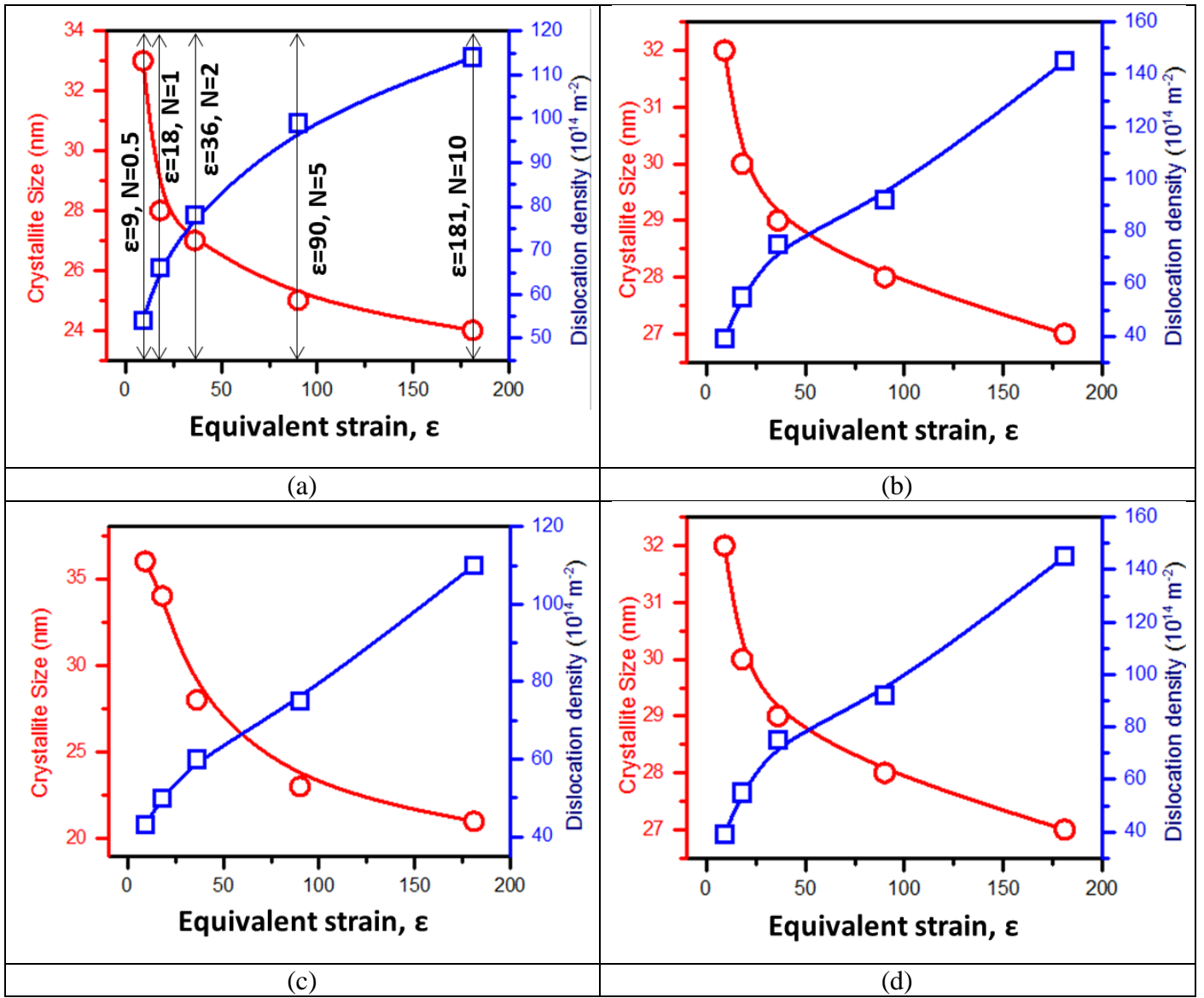


Figure 7: Variation in crystallite size and dislocation density with equivalent strain calculated from CMWP method for (a), (b) Ti64-C and Ti64+B-C alloys, respectively and (c), (d) Ti64-F and Ti64+B-F alloys, respectively. The equivalent strain, ϵ corresponding to various HPT-rotations are mentioned in (a).

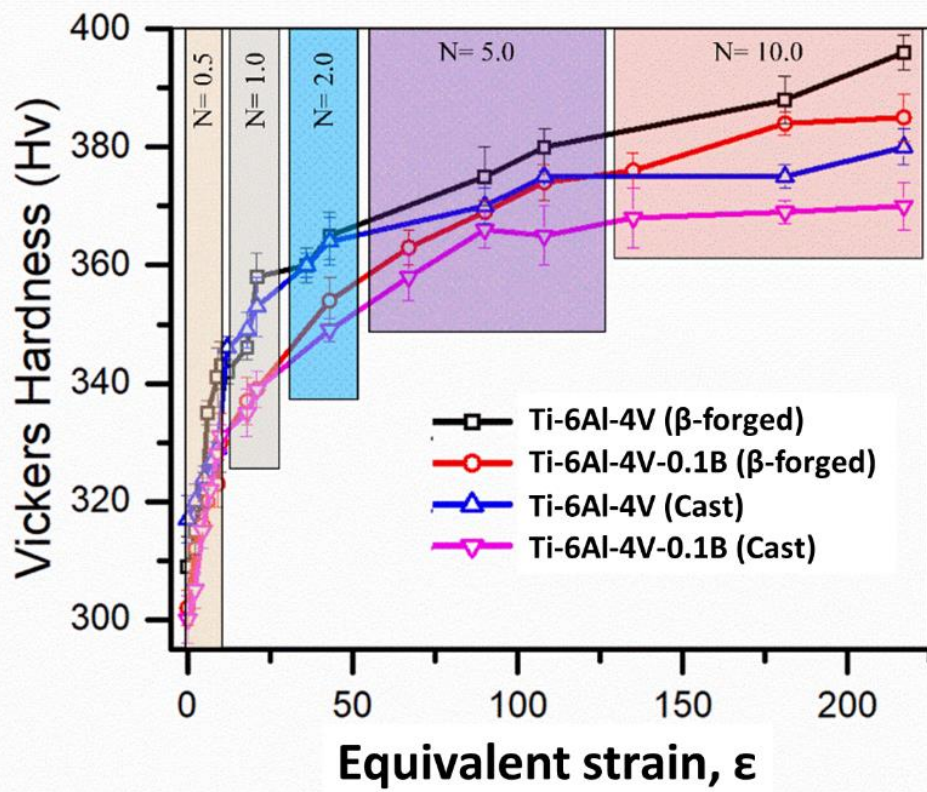


Figure 8: Hardness variation with equivalent strain for the alloys (unmodified and Boron modified) in different conditions (as-cast and β -forged).

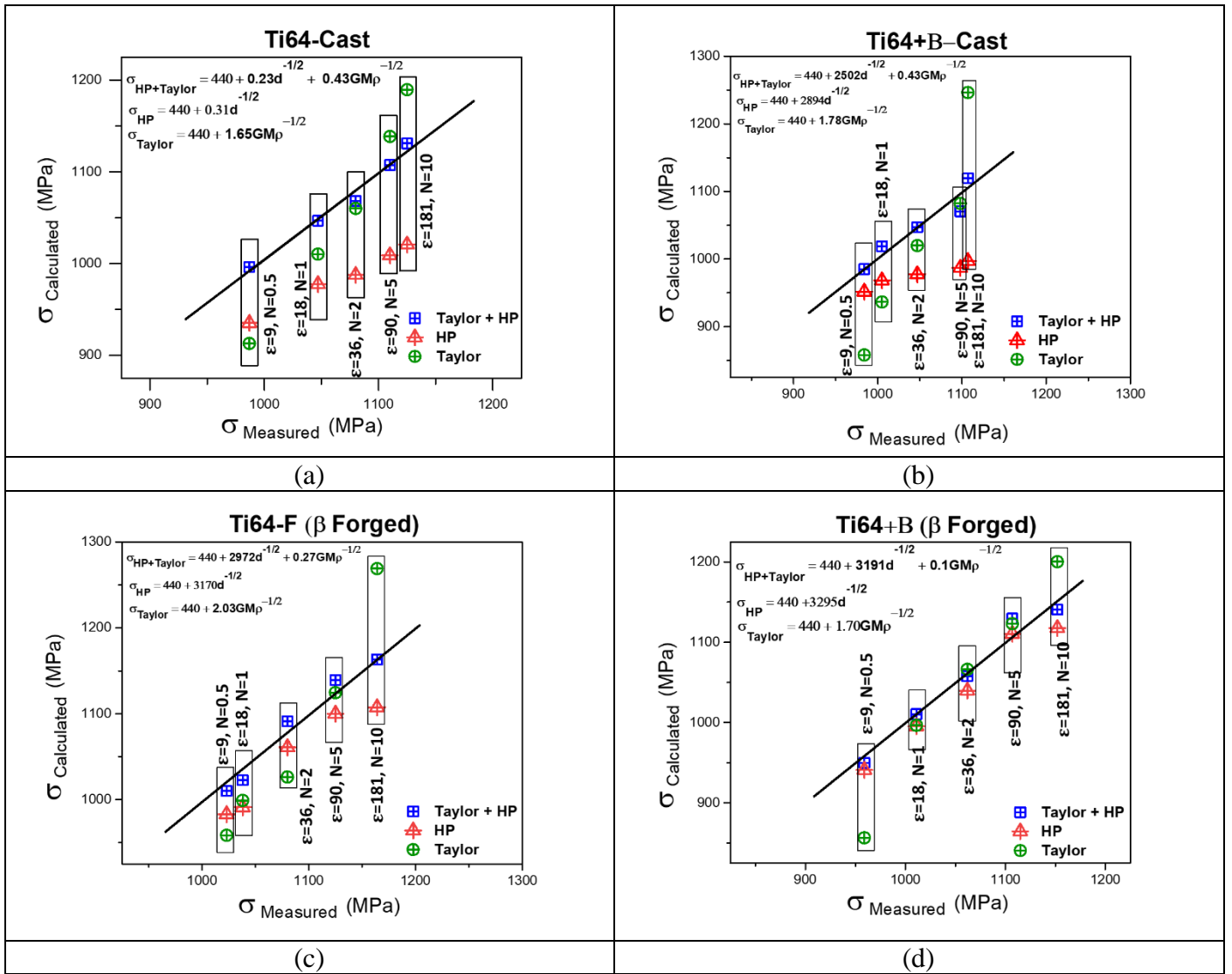


Figure 9: $\sigma_{measured}$ vs. $\sigma_{calculated}$ plots represent the contributions from various strengthening mechanisms towards strength increment (a) Ti64-C, (b) Ti64+B-C, (c) Ti64-F and (d) Ti64+B-F alloys.